Journal of Applied Physics

Improvements in graphene growth on 4H-SiC(0001) using plasma induced surface oxidation

Cite as: J. Appl. Phys. **126**, 065301 (2019); https://doi.org/10.1063/1.5092336
Submitted: 10 February 2019 . Accepted: 15 July 2019 . Published Online: 08 August 2019

Ouki Minami, Ryota Ito, Kohei Hosoo, Makoto Ochi, Yasuhisa Sano, Kentaro Kawai, Kazuya Yamamura, and Kenta Arima

Journal of Applied Physics ARTICLE scitation.org/journal/jap

Improvements in graphene growth on 4H-SiC (0001) using plasma induced surface oxidation

Cite as: J. Appl. Phys. **126**, 065301 (2019); doi: 10.1063/1.5092336
Submitted: 10 February 2019 · Accepted: 15 July 2019 ·
Published Online: 8 August 2019

Ouki Minami, Ryota Ito, Kohei Hosoo, Makoto Ochi, Yasuhisa Sano, Kentaro Kawai, Kazuya Yamamura, and Kenta Arima[a)]

AFFILIATIONS

Department of Precision Science and Technology, Graduate School of Engineering, Osaka University, 2-1, Yamada-oka, Suita, Osaka 565-0871, Japan

[a)]**Author to whom correspondence should be addressed:** arima@prec.eng.osaka-u.ac.jp

ABSTRACT

A Si-face 4H-SiC surface was modified by plasma oxidation followed by HF etching. The resulting surface was covered with a carbon overlayer composed of C–C bonded clusters and Si–O–C bonding from $Si_4C_4O_4$ and $Si_4C_{4-x}O_2$ ($x < 2$), as evidenced by photoemission spectroscopy measurements and wetting properties. A trend was observed in which the thickness of the carbon overlayer was proportional to the SiO_2 thickness after plasma oxidation, indicating that the former could be controlled on the subnanometer scale by adjusting plasma conditions. After a subsequent annealing under ultrahigh vacuum, we found that graphene grew on the modified SiC surface without the formation of a pitting morphology, which is in contrast to the case using an untreated SiC substrate. Raman spectroscopy revealed that the former graphene includes fewer defects than the latter graphene. We discuss the microscopic mechanism by which reaction products composed of C–C and Si–O–C bonds form in the SiO_2 film near the SiO_2/SiC interface via plasma oxidation as well as their influence on the subsequent growth of graphene.

I. INTRODUCTION

Graphene has drawn a considerable attention owing to its outstanding properties, such as electrical,[1] mechanical,[2] and magnetic[3] properties, which are expected to lead to numerous applications.[4] Various methods have been developed for obtaining graphene, including the mechanical exfoliation of graphite,[5] thermal decomposition of silicon carbide (SiC),[6–8] growth on metallic surfaces by chemical vapor deposition (CVD),[9] and chemical synthesis in solutions.[10] Among them, epitaxial growth of graphene on SiC has the advantage of forming large coherent graphene domains. In addition, SiC is a wide-bandgap semiconductor and can serve as a semi-insulating substrate, obviating the need to transfer graphene grown on SiC to another insulator substrate. These benefits have led to numerous reports on the synthesis of graphene via thermal sublimation of Si from SiC. The simplest technique is to heat a Si-face SiC surface in ultrahigh vacuum (UHV) to a temperature greater than 1100 °C, which results in Si sublimation.[6,8] However, a problem with this simple approach is the formation of a pitted morphology,[11,12] which is likely caused by the liberation of insufficient C atoms to form a uniform carbon-rich layer, the so-called "buffer layer," resulting in random sublimation of Si atoms from a terrace on SiC. The pitted morphology is likely to degrade the transport property of graphene,[13] which hampers further device development.

Thus far, various methods have been proposed to minimize etch pit formation during graphene growth. These approaches include the use of a vicinal SiC surface,[14] deposition of evaporated C atoms onto SiC,[15,16] rapid annealing of SiC,[17] selective etching of Si atoms in surface SiC layers by atomic hydrogen,[18] and the use of high background gas pressures during heating at temperatures above 1650 °C.[19] In this paper, we investigate the use of plasma to avoid a pitted morphology on SiC during subsequent heating in UHV to grow graphene.

Several groups have used plasma treatments of SiC for graphene growth.[20–25] For example, Raghavan *et al.* reported that the surface chemistry using CF_4- and Cl_2-based inductively coupled plasma-reactive ion etching of a SiC(0001) surface followed by thermal annealing has the potential to yield a large-area graphene film.[20] A C_4F_8-based fluorocarbon plasma was also used to etch a Si-face SiC surface prior to annealing in an Ar gas for nucleating

and growing graphene films.[21,22] Tsai *et al.* exposed a SiC surface to N_2 plasma to promote the reaction of nitrogen ions with Si, which was followed by annealing at 1150 °C in a N_2/H_2 atmosphere.[23] The objectives of these studies were to form graphene at lower temperatures than those required for simple Si sublimation. The plasma treatments were used for the selective removal of Si atoms from surface SiC layers, leaving a C-rich overlaying film as a carbon source on the surface. Zhang *et al.*[24] reported another approach of plasma-enhanced CVD using CH_4 as the carbon source. They achieved the epitaxial growth of graphene on SiC at controlled temperatures as low as ~540 °C during the CVD process.

In the present work, we use a novel surface chemical route to modify a SiC surface: plasma oxidation followed by wet etching. This sequence enables the condensation of carbon atoms on SiC with plasma that contains neither toxic nor flammable gases. We analyze the reaction products consisting of carbon species generated by these processes and discuss the mechanism of their synthesis. Then, the relationship between the SiO_2 thickness after plasma treatment and the carbon-containing overlayer thickness after the subsequent removal of the SiO_2 layer is revealed. We also show the influence of the carbon-rich overlayer on SiC on the quality of the graphene formed on such a surface.

II. EXPERIMENTAL DETAILS

A. Wet cleaning process

The samples used in this study were rectangles diced from chemical mechanical polished on-axis (±0.5°) 4H-SiC(0001) n-doped wafers. The nominal resistivity of these wafers was quoted as 0.015–0.028 Ω cm. The samples were first dipped into a solution of H_2SO_4/H_2O_2 (96 and 30 wt. %, respectively) = 4:1 (by volume) for 10 min to remove carbon and metallic contaminants on the surfaces. They were then dipped into a concentrated HF solution (50%) for 10 min, followed by being rinsed with ultrapure water for 10 min. The SiC surface after the wet cleaning procedure is referred to hereafter as the initial surface.

B. Plasma treatment

The initial surfaces after wet cleaning were treated with atmospheric-pressure plasma either in He or in a He/O_2 mixture. Figure 1 shows a schematic of our plasma apparatus. Samples with their initial surfaces were placed on a sample stage at room temperature, or 23 °C, in a chamber. After the air initially present in the chamber was evacuated by a dry scroll pump to a pressure of approximately 10 Pa, He was supplied until the chamber reached atmospheric pressure. A 6-mm-diameter cylindrical electrode was positioned above the sample surface at a distance of ~5 mm. When 150 MHz RF power (40 W) was applied to the electrode, atmospheric-pressure plasma was generated between the electrode and the sample surface, hereafter referred to as He-based plasma. In some experiments, we introduced a mixed gas of He and O_2 into the chamber, where the O_2 concentration was as high as 1.5%. The plasma with this mixed gas is herein referred to as the He/O_2 plasma. Considering the literature with the similar plasma conditions to ours,[26] the sample temperatures during these plasma

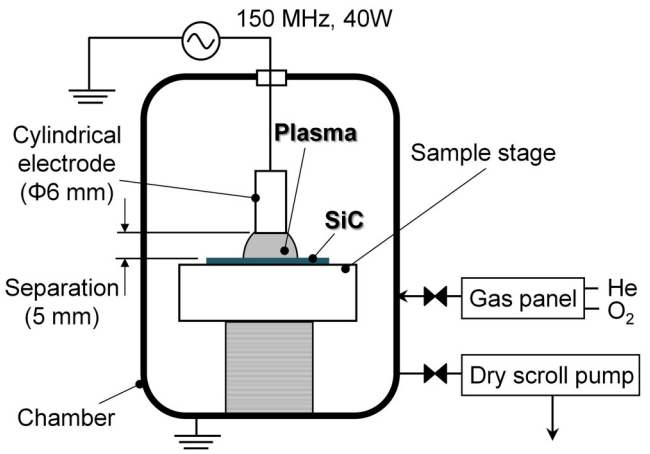

FIG. 1. Schematic of the plasma system.

treatments were expected to be lower than approximately 150 °C. The ion energy in our plasma was estimated to be not higher than several electron volts, meaning that we can avoid the mechanical damage of the SiC surface by the ion bombardment during the plasma exposure.

C. Graphene growth

The samples were immersed in a concentrated HF solution and rinsed with ultrapure water for 10 min after treatment with either He-based or He/O_2 plasma. The resulting surface is hereafter referred to as the modified surface. The samples with either the initial or modified surfaces were transferred to a chamber under UHV (2.0×10^{-8} Pa) and degassed at approximately 300 °C for 24 h. The samples were then heated from 300 °C to 1100 °C at a ramping rate of approximately 120 °C/s and maintained at 1100 °C for 30 min for the epitaxial growth of graphene on SiC. This heating process was carried out via direct-current heating. An optical pyrometer was used to monitor the temperature with an uncertainty of ±15 °C. Figure 2 summarizes our sample preparations.

D. Characterization and surface analysis

The obtained surfaces were analyzed by X-ray photoelectron spectroscopy (XPS, ULVAC-PHI, Quantum 2000), atomic force microscopy (AFM, Hitachi High-Tech Science, SPA-400) in tapping mode, and Raman spectroscopy (Nanophoton, RAMAN-touch). In the XPS spectra, the binding energy scale was calibrated using the Au $4f_{7/2}$ and Cu $2p_{3/2}$ lines. The Raman measurements were conducted with a 500-mW laser with a wavelength of 532 nm. The diameter of the spot size of the incident laser beam was 0.35 μm.

III. RESULTS AND DISCUSSION

Figure 3 shows peak-fitted XPS spectra on an initial SiC surface after the wet chemical treatment. The measured Si 2p spectrum in Fig. 3(a) has an intense peak at 101.3 eV from the SiC bulk

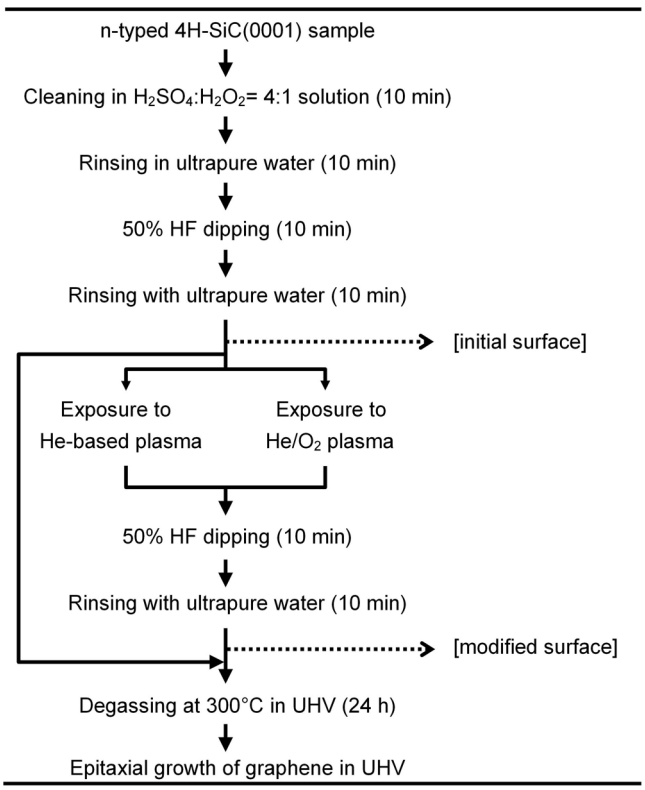

FIG. 2. Methods for the sample preparations.

together with a small shoulder peak, or the Si1 peak, at the higher-binding-energy side. In Fig. 3(b), a clear peak at 283.5 eV corresponds to C atoms bonded to Si in the SiC substrate. A small and broad component centered at 284.4 eV in Fig. 3(b) was attributed to surface carbon-containing species with an adventitious carbon component. The O 1s spectrum in Fig. 3(c) was almost fitted by a single peak at 532.8 eV. HF-treated SiC(0001) surfaces were previously shown to be terminated with OH groups.[27] The peak in Fig. 3(c) and the small Si1 peak in Fig. 3(a) likely represent surface hydroxyl groups bound to the outermost Si atoms. We placed a water droplet on this initial SiC surface. Figure 3(d) shows the corresponding image exhibiting more of a hydrophilic property caused by the OH groups terminating the SiC surface.

The graphs in Fig. 4 depict the XPS spectra of exposing the initial SiC surface to the He-based plasma. The Si 2p region in Fig. 4(a) includes two main peaks. One significant peak exists on the high-binding-energy side of the bulk peak and is attributed to an oxide (SiO_2) layer on SiC. The C 1s spectrum in Fig. 4(b) is composed of more lines than the Si spectrum. Specifically, in addition to the main peak from the SiC bulk at 283.5 eV, shoulder peaks situate at 284.4 eV (C1), 285.1 eV (C2), 286.0 eV (C3), and 287.1 eV (C4). According to the literature,[28,29] the C1, C2, C3, and C4 peaks are assigned to an interface oxide ($Si_4C_{4-x}O_2$; $x<2$), C–C bonded clusters, a mixed oxide ($Si_4C_4O_4$), and C–OH bonds, respectively. The C3 component also contains signals associated with hydrocarbon adsorbates.[28] The O 1s spectrum in Fig. 4(c) can be almost fitted with a single peak at 533.2 eV, which represents the formation of an SiO_2 layer. These results indicate that the SiC surface exposed to the He-based plasma was oxidized. The oxides originated from oxygen or water molecules remaining in the chamber, which led to the formation of oxidizing species such as oxygen and hydroxyl radicals. An emission spectrum revealed the presence of these radicals in the He-based plasma.[25] The graphs in Fig. 5 show the XPS spectra when the initial SiC surface was exposed to He/O_2 plasma with 1.5% O_2 concentration. A further surface oxidation occurred as manifested by the higher intensity ratio of the Si^{4+} signals to the SiC signals in the spectrum in Fig. 5(a) compared with that in Fig. 4(a). A feature in the C 1s spectrum in Fig. 5(b) has a low signal-to-noise ratio due to the presence of a thick SiO_2 layer attenuating the photoelectrons from the carbon species. The C 1s/Si 2p ratios were 0.17 and 0.06 in the spectra in Figs. 4 and 5, respectively. Note that the measured data in the C 1s region in Fig. 5(b) can be fitted by the same components as those in Fig. 4(b) (i.e., C1, C2, C3, and C4) together with a small and broad signal (C5) corresponding to COOH.[28]

Typical XPS spectra of a modified SiC surface are shown in Fig. 6. They were obtained after the sample exhibiting the spectra in Fig. 5 was removed from the XPS chamber and subsequently immersed into the concentrated HF solution, followed by being rinsed with ultrapure water. The oxide peak at approximately 103.7 eV in Fig. 5(a) disappears in Fig. 6(a), meaning that the SiO_2 layer was removed by the HF etchant. In Fig. 6(b), an intense shoulder emerges at a binding energy higher than the bulk peak at 283.3 eV. This shoulder was mainly fitted using the C2 and C3 peaks in Fig. 5(b) together with small contributions of C1 and C4. Evidence for Si–O–C bonding in the C3 ($Si_4C_4O_4$) and C1 ($Si_4C_{4-x}O_2$; $x<2$) components is also supported by the results in Fig. 6(c). Specifically, the O 1s spectrum in Fig. 6(c) can be deconvoluted into two peaks attributable to Si–O and C–O.[30] As noted in the discussion of Fig. 3(c), the Si–O signal is present after the HF treatment. Figures 6(b) and 6(c) indicate that our procedure created both C–C bonded clusters and Si–O–C bonding on a Si-face SiC surface. Table I summarizes the binding energy and the full-width half-maxima (FWHM) of the fitted peaks in Figs. 3–6. Table II compiles the relative contributions of C 1s and O 1s to Si 2p for each experiment. Figure 6(d) shows an image of the wetting property of a modified surface. As revealed in Fig. 6(d), the SiC surface with C–C and Si–O–C bonds exhibits greater hydrophobicity than the initial SiC surface covered with Si–O bonds [Fig. 3(d)]. Given the Pauling electronegativities of Si (1.90), C (2.55), and O (3.44) atoms, this change in wetting properties from Fig. 3(d) to Fig. 6(d) is reasonable. Another group reported the XPS spectra after the oxidation of a graphene/buffer layer/SiC structure.[31] According to their C 1s XPS spectra, the peak positions of graphene, a buffer layer [$(6\sqrt{3}\times 6\sqrt{3})R30^\circ$ phase], and an epoxy group in graphene oxide had a binding energy higher than the bulk SiC peak by 1.6, 2.4, and 3.2 eV, respectively. These peak positions were similar to those of C2, C3, and C4 in Fig. 6; hence, one may think that the modified surface in Fig. 6 represents graphene and graphene oxide coexisting on a buffer layer/SiC structure. However, the low-energy-electron-diffraction images on our modified surface

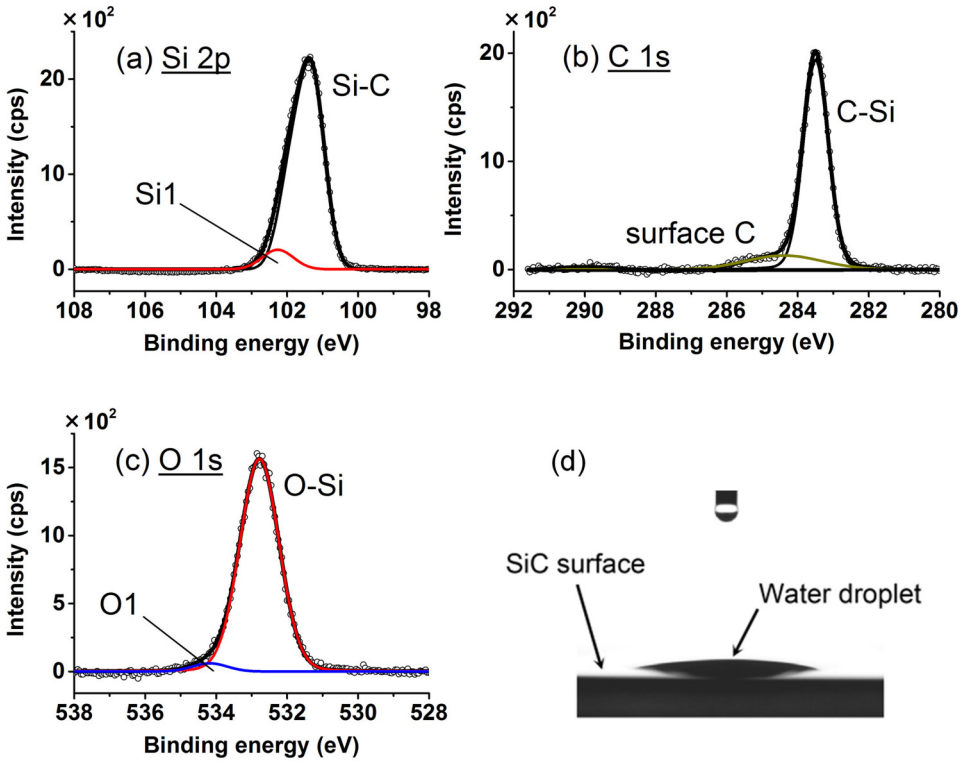

FIG. 3. (a) Si 2p, (b) C 1s, and (c) O 1s XPS spectra of an initial SiC surface. The photoelectron take-off angle was set to 20° from the sample surface. Cps in the label of the vertical axis is the abbreviation of counts per second. (d) Wetting property of this surface.

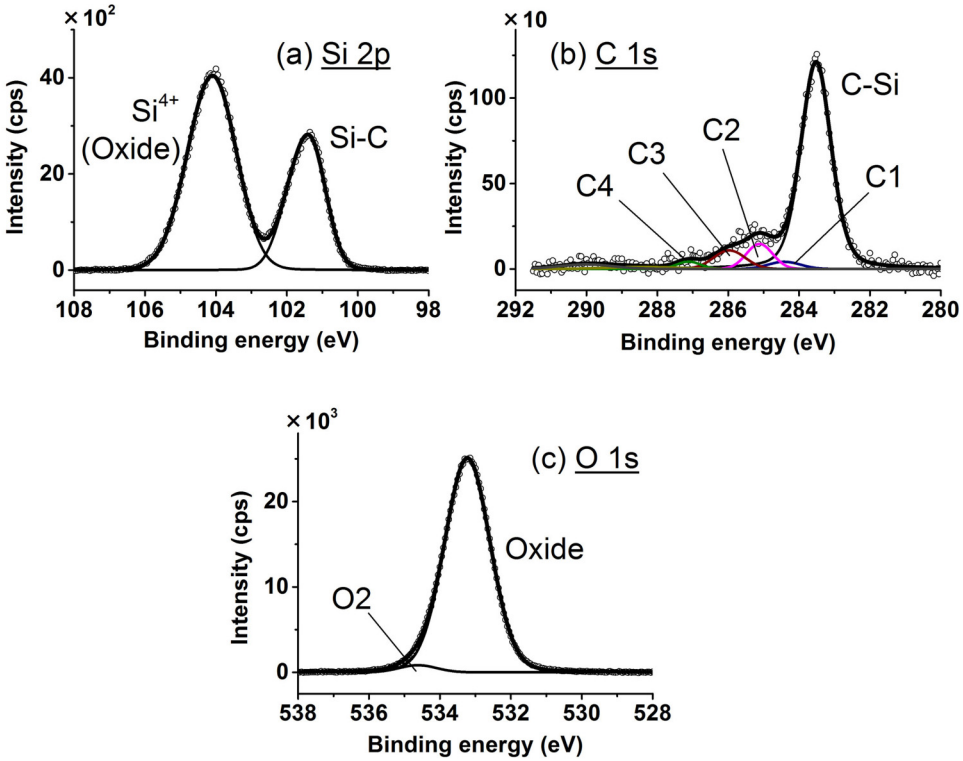

FIG. 4. (a) Si 2p, (b) C 1s, and (c) O 1s XPS spectra for the 90° take-off photoelectron emission angle for a SiC surface. They were obtained after an initial surface was exposed to the He-based plasma for 5 min.

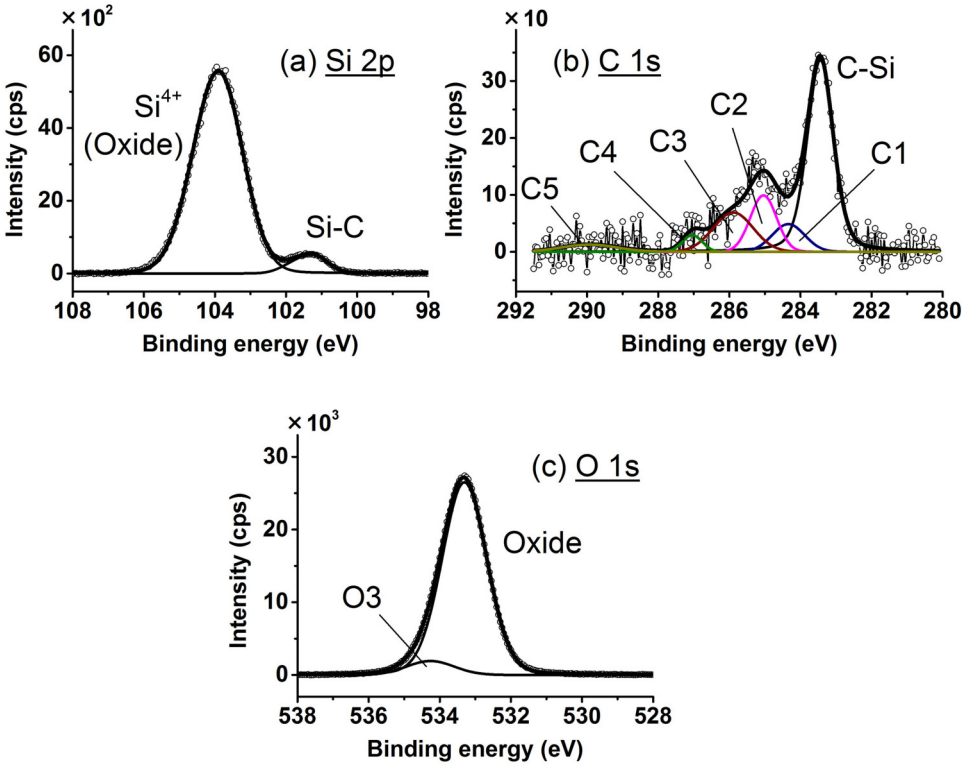

FIG. 5. (a) Si 2p, (b) C 1s, and (c) O 1s XPS spectra for the 90° take-off photoelectron emission angle for a SiC surface. These spectra were taken after an initial SiC surface was exposed to the He/O_2 plasma for 5 min. The O_2 concentration in the plasma was 1.5%. Note that the open symbols and the black bold curve indicate the measured data and the sum spectrum of the fitted peaks, respectively.

did not show any spots of either the buffer layer or graphene. Thus, we ruled out the possibility in which graphene or graphene oxide grew just by our plasma treatment of SiC followed by HF etching.

By analyzing the Si 2p and the C 1s spectra, we can estimate the thicknesses of SiO_2 and the carbon overlayer on SiC, respectively. Specifically, the SiO_2 thickness on the SiC substrate was calculated from the Si 2p signal attenuation using the equation[32]

$$t_{SiO_2} = \lambda_{SiO_2} \sin\theta \ln\left(\frac{N_{SiC}\lambda_{SiC}}{N_{SiO_2}\lambda_{SiO_2}}\frac{I_{SiO_2}}{I_{SiC}} + 1\right), \quad (1)$$

where I_{SiC} and I_{SiO_2} are the peak areas of the SiC bulk and SiO_2 in a Si 2p spectrum, N_{SiC} and N_{SiO_2} are the volume densities of Si atoms in the SiC bulk and SiO_2 film, λ_{SiC} and λ_{SiO_2} are the inelastic mean free paths of the photoelectrons in the SiC bulk and SiO_2 film, respectively, and θ is the electron take-off angle with respect to the sample surface. Using the values for N_{SiC} ($4.82 \times 10^{22}/cm^3$), N_{SiO_2} ($2.21 \times 10^{22}/cm^3$), λ_{SiC} (2.615 nm), and λ_{SiO_2} (3.764 nm) found in the literature,[33–35] for example, we obtained SiO_2 thicknesses of 5.0 nm and 14 nm for the spectra in Figs. 4(a) and 5(a), respectively.

Similarly, the thickness of a carbon-containing overlayer on SiC can be estimated from the C 1s spectra. As described in Fig. 6, the carbon-containing overlayer has multiple components, including C–C bonded clusters and intermediate oxides. For simplicity, we regarded the volume density of the C atoms ($1.14 \times 10^{23}/cm^3$) and the inelastic mean free path of the photoelectrons in the carbon-containing overlayer (3.714 nm) as those reported in the literature for glassy carbon.[36,37] Moreover, 2.344 nm was used for the inelastic mean free path of the photoelectrons from the C 1s orbital in the SiC bulk.[33] In this manner, the C 1s spectrum [Fig. 6(b)] was shown to have an overlayer with a thickness of 0.26 nm.

We next investigated the relationship between the SiO_2 and carbon-overlayer thicknesses for four different plasma conditions by analyzing the Si 2p and C 1s XPS spectra. We employed both the He-based and He/O_2 plasma. The latter was used to control the O_2 concentration in the chamber. Figure 7(a) shows that increasing the O_2 concentration in the He/O_2 plasma resulted in a thicker SiO_2 film. This result is reasonable because O_2 molecules are the source of oxidizing species in the plasma. The more important trend is that a thicker oxide film on SiC created a thicker carbon overlayer, as shown in Fig. 7(b). For example, when the oxide thicknesses were 6.6 nm and 12.6 nm, the carbon-overlayer thicknesses after the subsequent HF etching were 0.16 nm and 0.29 nm, respectively. Figure 7(b) indicates that the thickness of the additional carbon layer can be controlled on the subnanometer scale by controlling oxide thicknesses.

A mechanism to form the C–C bonded clusters in the carbon-containing overlayer, which caused the C2 peak in Figs. 4(b) and 5(b), is proposed as follows. In conventional thermal oxidation of SiC at temperatures in the range between 1100 and 1400 °C, gaseous CO molecules are generated by the reaction $2SiC(s) + 3O_2(g) \rightarrow 2SiO_2(s) + 2CO(g)$.[38] Because CO molecules in SiO_2 can

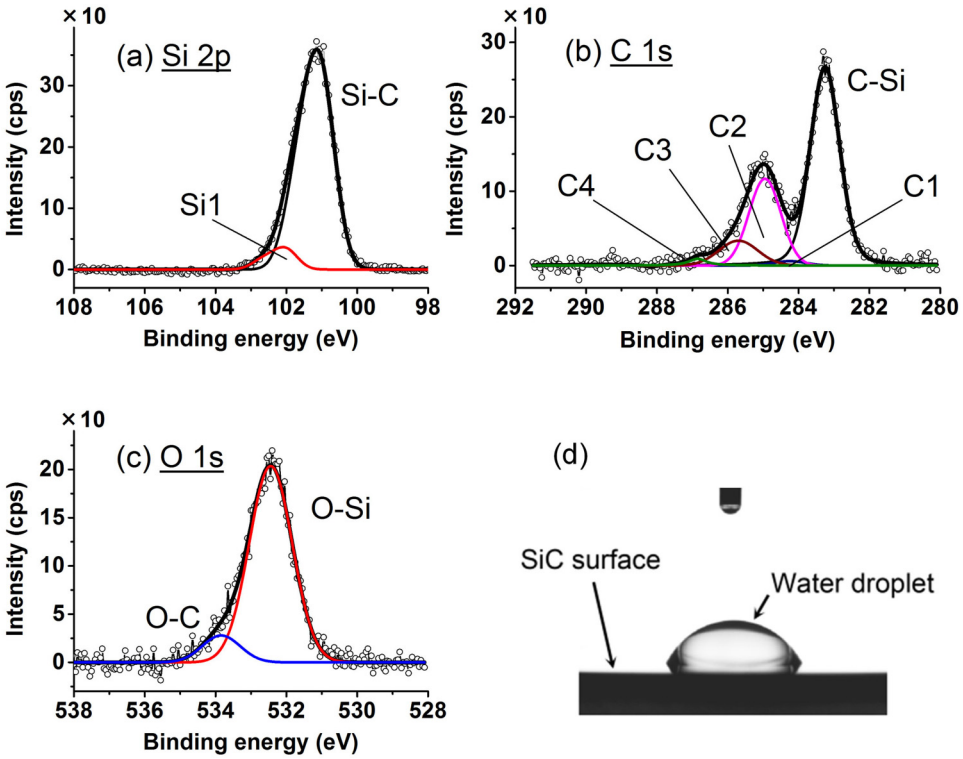

FIG. 6. (a) Si 2p, (b) C 1s, and (c) O 1s XPS spectra for 20° take-off photoelectron emission of a modified SiC surface. These spectra were collected after the SiO_2 layer of the sample represented in Fig. 5 was removed by HF etching. (d) Wetting property of a modified surface.

be emitted in the gas phase at temperatures greater than 900 °C,[39] they do not reside at the SiO_2/SiC interface, as also confirmed in the literature.[40] By contrast, our plasma oxidized the SiC sample at temperature lower than 150 °C. Even if CO molecules are generated by the interaction of SiC with oxidizing species, the oxidation temperature is too low for CO to diffuse into the SiO_2 layer. As a result, the CO molecules are likely to remain, especially at the SiO_2/SiC interface, and to aggregate to form O-deficient carbon clusters containing the C–C bonds via the effusion of O atoms as CO_2.[41] The formation of carbon precipitates during thermal oxidation was also investigated from the viewpoint of thermodynamics.[38,42] At a given O_2 partial pressure, the reaction of O_2 with SiC results in different products depending on the temperature. Carbon precipitation $[SiC(s) + O_2(g) \rightarrow SiO_2(s) + C(s)]$, rather than the generation of gaseous CO molecules, is thermodynamically favored in low-temperature regions. In addition, the C1 and C3 peaks representing $Si_4C_{4-x}O_2$ and $Si_4C_4O_4$ in Figs. 4(b) and 5(b) were considered to be a reaction product of the molecular O_2 bonded peroxidically to a SiC bilayer and an oxidation product of $Si_4C_{4-x}O_2$, respectively.[28] Although we need further investigations, the formation of the carbon species (C–C bonded clusters, interface oxide, and mixed oxide) is likely caused by a low oxidation temperature (i.e., a temperature lower than 150 °C). These species remained after HF etching of the SiO_2 layer to form an overlayer containing the C–C and Si–O–C bonds on the modified surface [Fig. 6(b)].

Figure 8 shows the change in surface morphologies of different SiC samples as a result of the UHV annealing process. The initial SiC surface is composed of atomically flat terraces and step edges, as shown in Fig. 8(a). In this image, the terrace width is approximately 230 nm, although it could vary in the range between 90 and 250 nm even on the same wafer surface because of the local variations. The step height in Fig. 8(a) was 0.25 nm, which corresponds to the single bilayer of the SiC crystal. Figures 8(b)–8(d) show the modified SiC surfaces. The initial terrace/step structure in Fig. 8(a) became unclear, and its extent was more significant on the samples exposed longer to the He-based plasma. In another experiment, we confirmed that the thickness of the carbon overlayer composed of the C–C bonded clusters and the Si–O–C bonds presented in Figs. 6 and 7 increased with increasing plasma exposure time. The AFM images in Figs. 8(b)–8(d) indicate that a thicker carbon overlayer covers the underlying SiC surface more completely, which is also evidenced by the change in the root-mean-square roughness provided for each image. After the heat treatment under UHV, the surface morphologies changed from those in Fig. 8(a) to those in Fig. 8(e). As evident in Fig. 8(e), many pits, whose depths were measured to be 1.0–1.5 nm, were formed. Another group has reported AFM phase images that reveal the presence of graphene layers even at the bottom of these pits.[43] Figure 8(f) was obtained when graphene was epitaxially grown on the SiC sample shown in Fig. 8(b). The pit density is apparently lower in Fig. 8(f) than in Fig. 8(e), and this trend is more clearly observed on the graphene/SiC structures in Figs. 8(g) and 8(h). The carbon overlayer on SiC observed in Figs. 8(b)–8(d) can be reasonably considered to contribute to the suppression of the formation of the pitted morphology. Notably, the step edges in Figs. 8(g) and 8(h) are straighter than those in Figs. 8(e) and 8(f).

TABLE I. Description of the spectra fitting for Figs. 3–6.

Figure	Components	Binding energy (eV)	FWHM (eV)
		Si $2p^{3/2}$	
3	Si–C	101.3	0.8
3	Si1	102.3	1.0
4	Si–C	101.3	1.0
4	Oxide	103.9	1.5
5	Si–C	101.2	0.9
5	Oxide	103.7	1.5
6	Si–C	101.0	0.9
6	Si1	102.0	0.8
		C 1s	
3	C–Si	283.5	0.8
3	Surface C	284.4	2.3
4	C–Si	283.5	1.0
4	C1	284.4	1.1
4	C2	285.1	0.9
4	C3	286.0	1.1
4	C4	287.1	0.8
5	C–Si	283.4	0.9
5	C1	284.3	1.1
5	C2	285.0	0.9
5	C3	285.9	1.3
5	C4	287.0	0.7
5	C5	289.9	1.8
6	C–Si	283.3	1.0
6	C1	284.3	1.1
6	C2	285.0	1.1
6	C3	285.7	1.3
6	C4	286.9	0.6
		O 1s	
3	O–Si	532.8	1.3
3	O1	534.2	1.2
4	Oxide	533.2	1.5
4	O2	534.6	1.2
5	Oxide	533.3	1.5
5	O3	534.3	1.6
6	O–Si	532.4	1.4
6	O–C	533.8	1.3

Figure 9 presents the Raman spectra collected to evaluate the influence of the plasma-assisted process on the quality of graphene. We prepared two samples. One was an as-received SiC surface cleaned with a mixed solution of H_2SO_4 and H_2O_2. The other was a SiC surface exposed to the He-based plasma for 5 min. After the immersion of these surfaces into the concentrated HF solution, followed by rinsing with ultrapure water, graphene was grown on the SiC surfaces in UHV in the manner in Sec. II C. For each sample, 36 Raman spectra were collected and a background signal was subtracted. The averaged spectra for the modified and the initial SiC surfaces are shown in Figs. 9(a) and 9(b), respectively.

TABLE II. Summary of the C 1s/Si 2p and O 1s/Si 2p data for Figs. 3–6. The peak areas are not corrected by the sensitivity factors.

Figure	C 1s/Si 2p	O 1s/Si 2p	Photoemission take-off angle (deg)
3	0.73	0.82	20
4	0.17	3.98	90
5	0.06	4.44	90
6	1.01	0.71	20

The major features of Raman spectra of graphene are the D peak at ~1350 cm^{-1}, the G peak at ~1584 cm^{-1}, and the 2D peak at ~2700 cm^{-1}. The G peak is related to phonon vibrations in sp^2 carbon materials, whereas the 2D peak is a second-order two-phonon mode. The D peak is not Raman active for pristine graphene but can be detected when the symmetry of graphene is broken either by outer edges or by a high density of defects.[44] In

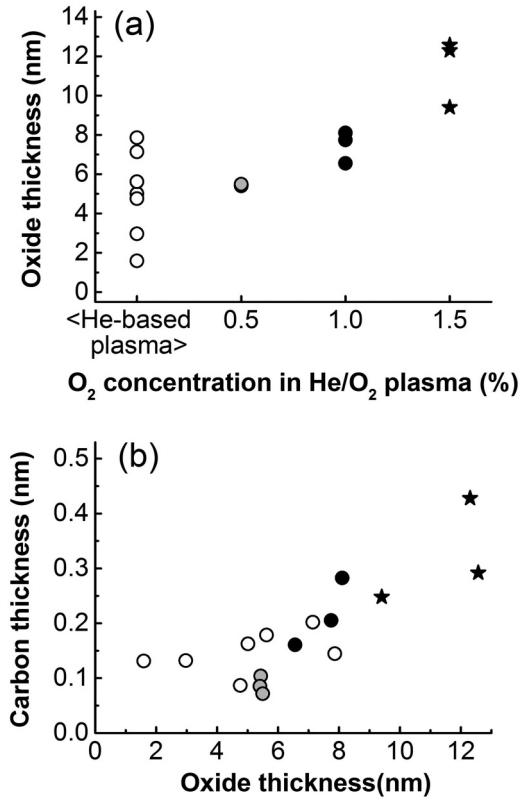

FIG. 7. (a) SiO_2 thicknesses as a function of the O_2 concentrations in the He/O_2 plasma. The open symbols represent the data with the He-based plasma. Each plot was obtained when an initial SiC surface was exposed to plasma for 5 min. (b) Thicknesses of a carbon overlayer on modified SiC as a function of the SiO_2 thicknesses. After removing the SiO_2 layer by HF etching, the carbon layer thickness was estimated by taking a C 1s XPS spectrum. The definitions of the symbols are the same as those in (a).

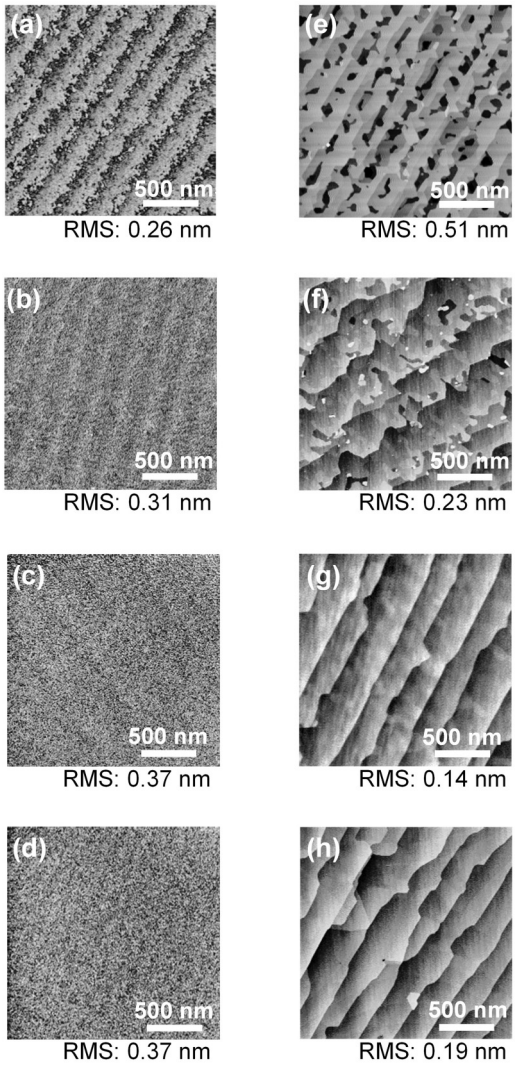

FIG. 8. AFM images of SiC surfaces. (a) Initial surface after wet cleaning. (b)–(d) Modified SiC surfaces. Prior to the immersion into concentrated HF, the samples were treated with the He-based plasma for 1 min, 5 min, and 10 min, respectively. (e), (f), (g), and (h) are the surfaces of graphene/SiC structures after the heat treatment of the sample in (a), (b), (c), and (d) at 1100 °C for 30 min under UHV, respectively. Root-mean-square (RMS) roughness is provided for each image.

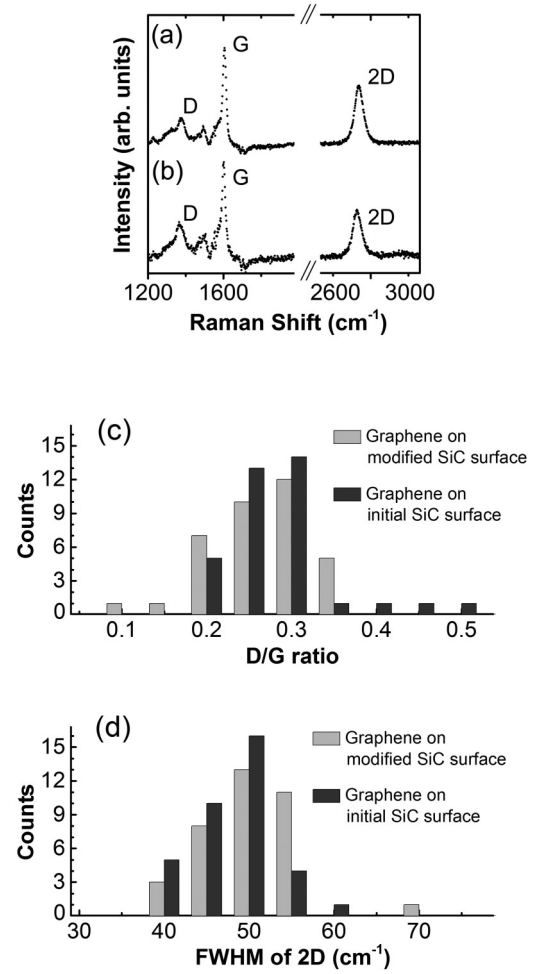

FIG. 9. Raman spectra of two different graphene/SiC structures. A total of 36 Raman spectra were recorded for each sample. (a) and (b) Average of the 36 spectra of graphene grown on the modified and the initial SiC surfaces, respectively. (c) and (d) The frequency distribution of the D/G ratio and the full-width at half-maximum of a 2D peak, respectively.

general, as the size of the graphene crystallites is reduced, more disorder is introduced and the D/G ratio increases.[45] We found that the intensity of the D peak in Fig. 9(a) is weaker than that in Fig. 9(b). For clarity, the frequency distributions of the D/G ratio for both samples are shown in Fig. 9(c). The D/G ratios of graphene grown on the modified SiC are less than 0.35, whereas they exceed 0.4 for several spectra of graphene grown on the initial SiC. The formation of graphene with a lower defect density on the modified SiC than on the initial one is reasonable.

The FWHM value of a 2D peak is widely used to estimate the graphene thickness. Specifically, the FWHM values of monolayer and bilayer graphene on the Si-face SiC have been reported to be approximately 40 and 60 cm^{-1}, respectively.[46] Figure 9(d) is the FWHM frequency distribution among the 36 spectra for each sample. For both samples, most of the FWHM values are in the range between 40 and 55 cm^{-1}, meaning that mono- and bilayer graphene coexist. That is, the results in Fig. 9(d) insist that the number of graphene layers is similar between the two samples.

Figure 10 depicts graphene grown on two different SiC surfaces. For samples subjected to elevated temperatures under UHV, step edges become unstable and begin to release both Si and C atoms. Because of the difference in the vapor pressures of Si and C atoms, Si atoms are desorbed from the surface, whereas C atoms

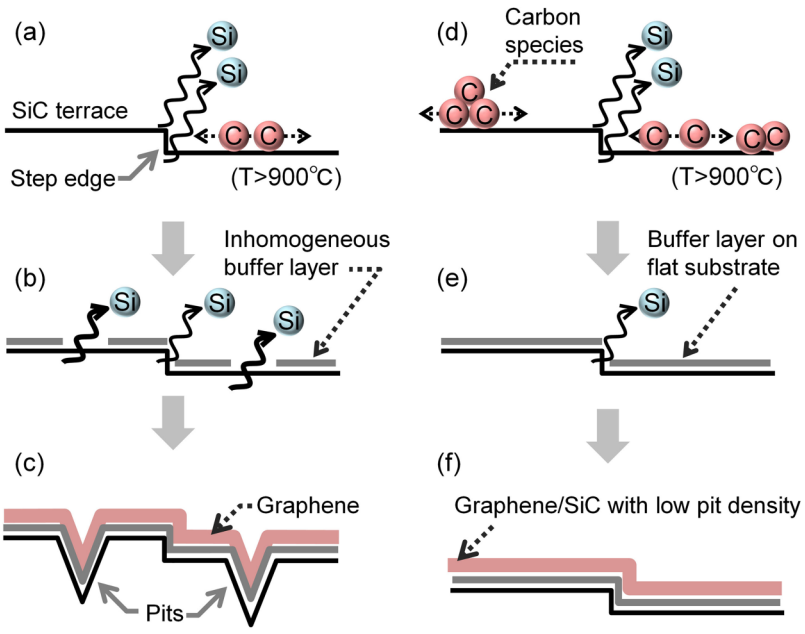

FIG. 10. Schematic of graphene growth on SiC(0001). The heat treatment was assumed to be conducted on two different surfaces: [(a)–(c)] the initial SiC surface and [(d)–(f)] the modified surface with a carbon overlayer. As shown in (a) and (d), the sublimation of Si atoms starts at temperatures higher than 900 °C under UHV. (b) and (e) depict that surface C atoms first form a buffer layer. When the concentration of surface C atoms is too low to form a uniform buffer layer, random sublimation of Si atoms occurs from terraces, as shown in (b). (c) and (f) illustrate that graphene is formed at temperatures above 1100 °C.

migrate on the surface to form the $(6\sqrt{3} \times 6\sqrt{3})R30^\circ$ buffer layer, as shown in Fig. 10(a).[47,48] However, if the amount of C atoms is insufficient, this buffer layer does not cover the entire surface. As Fig. 10(b) illustrates, this scenario leads to the random sublimation of Si atoms from the terrace not covered by the buffer layer, although the SiC surface under the buffer layer becomes thermally stable. As a result, graphene grows on the pitted morphology at higher temperatures above 1100 °C, as shown in Fig. 10(c). Figures 10(a)–10(c) present the graphene growth process on the initial SiC surface. By contrast, the modified surface has a carbon overlayer composed of C–C bonded clusters and other species, such as oxides [i.e., $Si_4C_4O_4$ and $Si_4C_{4-x}O_2$ $(x < 2)$] and C–H bonding from hydrocarbons, as discussed earlier. This overlayer probably acts as a barrier layer that limits Si evaporation and reduces pit formation, which assists the formation of a buffer layer on a flat SiC surface at temperatures above 900 °C as schematically depicted in Figs. 10(d) and 10(e). King *et al.* have reported that adventitious carbon, or hydrocarbon contaminants composed of C–H and C–O mixtures, is desorbed after UHV annealing at 800 °C.[29] Thus, we speculate that hydrocarbon adsorbates on the modified SiC surface, which represents part of the C3 peak in Fig. 6(b), are not a carbon source to form the uniform buffer layer. However, the fate of the oxides ($Si_4C_4O_4$ and $Si_4C_{4-x}O_2$) at elevated temperatures is not clear. They likely decomposed at temperatures above approximately 900 °C. The resulting carbon atoms as well as the C–C bonded clusters in the overlayer may become a carbon source to form the buffer layer.[15,16] Further investigation is necessary to elucidate the behavior of carbon species consisting of the carbon overlayer at high temperatures under UHV. In any event, graphene is likely to grow on such a flat SiC surface, as depicted in Fig. 10(f). This ease of growth is why the graphene/SiC structure with low pit densities is formed in Figs. 8(g) and 8(h). Graphene grown on step edges is known to contain a high density of structural defects;[49] our results in Figs. 9(a)–9(c), which show that graphene with a lower defect density formed on the modified SiC than on the initial one, are, therefore, reasonable. Finally, more Si atoms are sublimated in Fig. 10(b) than in Fig. 10(e), and the sublimation process accompanies the creation of more C atoms on a pitted SiC. As a result, the amount of carbon atoms liberated to form graphene at approximately 1100 °C may be similar between the two samples. Such similarity would explain the results in Fig. 9(d), where the carbon overlayer on SiC before heating does not substantially affect the number of graphene layers.

IV. CONCLUSIONS

A thermal treatment under UHV is a simple and familiar method for the epitaxial growth of graphene on SiC surfaces. However, the formation of a pitting morphology is inevitable and numerous investigators have attempted to address this problem. We proposed herein a plasma treatment to modify a Si-face SiC surface, which has the potential to eliminate the problem. Carbon species, such as C–C bonded clusters and an interface oxide ($Si_4C_{4-x}O_2$; $x < 2$), were formed after plasma oxidation at a temperature lower than 150 °C. The origin of the C–C and Si–O–C species was discussed on the basis of oxidation products depending on temperatures and thermodynamics. We then investigated the relationship between SiO_2 thickness and a carbon-overlayer thickness after subsequent removal of the SiO_2 layer. We annealed the modified SiC surface with an additional carbon overlayer to form graphene under UHV. The resultant graphene/SiC structure included a low pit density. The carbon overlayer was supposed to serve as a barrier layer that limits the large-scale Si evaporation and the accompanying pit formation, which enabled us to form

graphene on a flat SiC surface. Raman spectroscopy also revealed that this graphene included fewer defects than that on an untreated SiC surface. As shown in this study, a plasma treatment may open new chemical routes to form two-dimensional materials with better characteristics than those used today.

ACKNOWLEDGMENTS

This work was supported by the Japan Society for the Promotion of Science (JSPS) KAKENHI under Grant No. JP15H03902. This work was also supported in part by the SEI Group CSR Foundation. A part of this work was supported by "Nanotechnology Platform Project (Nanotechnology Open Facilities in Osaka University)" of Ministry of Education, Culture, Sports, Science and Technology, Japan (Nos. S-19-OS-0005 and F-19-OS-0009).

REFERENCES

[1]A. K. Geim and K. S. Novoselov, Nat. Mater. **6**, 183–191 (2007).
[2]I. W. Frank, D. M. Tanenbaum, A. M. van der Zande, and P. L. McEuen, J. Vac. Sci. Technol. B **25**(6), 2558–2561 (2007).
[3]D. Xiao, W. Yao, and Q. Niu, Phys. Rev. Lett. **99**(23), 236809 (2007).
[4]I. Shtepliuk, V. Khranovskyy, and R. Yakimova, Semicond. Sci. Technol. **31**(11), 113004 (2016).
[5]K. S. Novoselov, A. K. Geim, S. V. Morozov, D. Jiang, Y. Zhang, S. V. Dubonos, I. V. Grigorieva, and A. A. Firsov, Science **306**(5696), 666–669 (2004).
[6]A. J. Van Bommel, J. E. Crombeen, and A. Van Tooren, Surf. Sci. **48**(2), 463–472 (1975).
[7]C. Berger, Z. Song, T. Li, X. Li, A. Y. Ogbazghi, R. Feng, Z. Dai, A. N. Marchenkov, E. H. Conrad, P. N. First, and W. A. de Heer, J. Phys. Chem. B **108**(52), 19912–19916 (2004).
[8]R. M. Tromp and J. B. Hannon, Phys. Rev. Lett. **102**(10), 106104 (2009).
[9]J. Wintterlin and M. L. Bocquet, Surf. Sci. **603**(10), 1841–1852 (2009).
[10]S. Park and R. S. Ruoff, Nat. Nanotechnol. **4**, 217–224 (2009).
[11]G. Gu, S. Nie, R. M. Feenstra, R. P. Devaty, W. J. Choyke, W. K. Chan, and M. G. Kane, Appl. Phys. Lett. **90**(25), 253507 (2007).
[12]J. B. Hannon and R. M. Tromp, Phys. Rev. B **77**(24), 241404 (2008).
[13]S.-H. Ji, J. B. Hannon, R. M. Tromp, V. Perebeinos, J. Tersoff, and F. M. Ross, Nat. Mater. **11**, 114–119 (2012).
[14]G. F. Sun, Y. Liu, S. H. Rhim, J. F. Jia, Q. K. Xue, M. Weinert, and L. Li, Phys. Rev. B **84**(19), 195455 (2011).
[15]A. Al-Temimy, C. Riedl, and U. Starke, Appl. Phys. Lett. **95**(23), 231907 (2009).
[16]J. Park, W. C. Mitchel, L. Grazulis, H. E. Smith, K. G. Eyink, J. J. Boeckl, D. H. Tomich, S. D. Pacley, and J. E. Hoelscher, Adv. Mater. **22**(37), 4140–4145 (2010).
[17]M. Hupalo, E. H. Conrad, and M. C. Tringides, Phys. Rev. B **80**(4), 041401 (2009).
[18]A. Sandin, J. E. Rowe, and D. B. Dougherty, Surf. Sci. **611**, 25–31 (2013).
[19]K. V. Emtsev, A. Bostwick, K. Horn, J. Jobst, G. L. Kellogg, L. Ley, J. L. McChesney, T. Ohta, S. A. Reshanov, J. Rohrl, E. Rotenberg, A. K. Schmid, D. Waldmann, H. B. Weber, and T. Seyller, Nat. Mater. **8**(3), 203–207 (2009).
[20]S. Raghavan, T. J. Denig, T. C. Nelson, and C. D. Stinespring, J. Vac. Sci. Technol. B **30**(3), 030605 (2012).
[21]Y. Xu, X. Wu, C. Ye, Y. Deng, T. Chen, and S. Ge, Thin Solid Films **527**, 65–68 (2013).
[22]C. G. Jin, T. Y. Huang, Y. Yang, M. Z. Wu, Y. J. Xu, Z. F. Wu, L. J. Zhuge, X. M. Wu, and C. Ye, Plasma Process. Polym. **12**(10), 1061–1068 (2015).
[23]H.-S. Tsai, C.-C. Lai, H. Medina, S.-M. Lin, Y.-C. Shih, Y.-Z. Chen, J.-H. Liang, and Y.-L. Chueh, Nanoscale **6**(22), 13861–13869 (2014).
[24]L. C. Zhang, Z. W. Shi, D. H. Liu, R. Yang, D. X. Shi, and G. Y. Zhang, Nano Res. **5**(4), 258–264 (2012).
[25]N. Saito, D. Mori, A. Imafuku, K. Nishitani, H. Sakane, K. Kawai, Y. Sano, M. Morita, and K. Arima, Carbon **80**, 440–445 (2014).
[26]Y. Sano, M. Watanabe, T. Kato, K. Yamamura, H. Mimura, and K. Yamauchi, Mater. Sci. Forum **600–603**, 847–850 (2009).
[27]U. Starke, C. Bram, P. R. Steiner, W. Hartner, L. Hammer, K. Heinz, and K. Müller, Appl. Surf. Sci. **89**(2), 175–185 (1995).
[28]B. Hornetz, H. J. Michel, and J. Halbritter, J. Mater. Res. **9**(12), 3088–3094 (1994).
[29]S. W. King, S. Tanaka, R. F. Davis, and R. J. Nemanich, J. Vac. Sci. Technol. A **33**(5), 05E105 (2015).
[30]S. W. King, R. J. Nemanich, and R. F. Davisa, J. Electrochem. Soc. **146**(5), 1910–1917 (1999).
[31]E. Velez-Fort, A. Ouerghi, M. G. Silly, M. Eddrief, A. Shukla, F. Sirtti, and M. Marangolo, Appl. Phys. Lett. **104**(9), 093109 (2014).
[32]T. A. Carlson, Surf. Interface Anal. **4**(4), 125–134 (1982).
[33]S. Tanuma, C. J. Powell, and D. R. Penn, Surf. Interface Anal. **17**(13), 927–939 (1991).
[34]G. W. C. Kaye and T. H. Laby, *Tables of Physical and Chemical Constants* (Longmans, New York, 1995).
[35]A. Gomes, Acta Crystallogr. **23**(4), 610–617 (1967).
[36]M. P. Seah and S. J. Spencer, J. Vac. Sci. Technol. A **21**(2), 345–352 (2003).
[37]B. Lesiak, A. Jablonski, Z. Prussak, and P. Mrozek, Surf. Sci. **223**(1–2), 213–232 (1989).
[38]R. H. Kikuchi and K. Kita, Appl. Phys. Lett. **105**(3), 032106 (2014).
[39]C. Köhler, Z. Hajnal, P. Deák, T. Frauenheim, and S. Suhai, Phys. Rev. B **64**(8), 085333 (2001).
[40]H. Watanabe, T. Hosoi, T. Kirino, Y. Kagei, Y. Uenishi, A. Chanthaphan, A. Yoshigoe, Y. Teraoka, and T. Shimura, Appl. Phys. Lett. **99**, 021907 (2011).
[41]S. Wang, M. Di Ventra, S. G. Kim, and S. T. Pantelides, Phys. Rev. Lett. **86**(26), 5946–5949 (2001).
[42]Y. Song and F. W. Smith, Appl. Phys. Lett. **81**(16), 3061–3063 (2002).
[43]D. Ferrah, J. Penuelas, C. Bottela, G. Grenet, and A. Ouerghi, Surf. Sci. **615**, 47–56 (2013).
[44]M. J. Allen, V. C. Tung, and R. B. Kaner, Chem. Rev. **110**(1), 132–145 (2010).
[45]L. G. Cançado, K. Takai, T. Enoki, M. Endo, Y. A. Kim, H. Mizusaki, A. Jorio, L. N. Coelho, R. Magalhães-Paniago, and M. A. Pimenta, Appl. Phys. Lett. **88**(16), 163106 (2006).
[46]D. S. Lee, C. Riedl, B. Krauss, K. von Klitzing, U. Starke, and J. H. Smet, Nano Lett. **8**(12), 4320–4325 (2008).
[47]W. Norimatsu, J. Takada, and M. Kusunoki, Phys. Rev. B **84**(3), 035424 (2011).
[48]S. Tanaka, K. Morita, and H. Hibino, Phys. Rev. B **81**(4), 041406 (2010).
[49]J. Robinson, X. Weng, K. Trumbull, R. Cavalero, M. Wetherington, E. Frantz, M. LaBella, Z. Hughes, M. Fanton, and D. Snyder, ACS Nano **4**(1), 153–158 (2010).